

Exact-Diagonalization Studies of Inelastic Light Scattering in Self-Assembled Quantum Dots

Alain Delgado^a, Adriel Domínguez^b, Ricardo Pérez^c, D.J. Lockwood^d, and Augusto González^e

^a Centro de Aplicaciones Tecnológicas y Desarrollo Nuclear,
Calle 30 No 502, Miramar, Ciudad Habana, C.P. 11300, Cuba

^b Instituto Superior de Tecnologías y Ciencias Aplicadas,
Quinta de los Molinos, Ciudad Habana, C.P. 10600, Cuba

^c Depment. of Eng. Phys., McMaster University, Ontario, Canada L8S 4L7

^d Institute for Microstructural Sciences, National Research Council,
1200 Montreal Road, Ottawa, Ont., Canada K1A 0R6

^e Instituto de Cibernética, Matemática y Física, Calle E 309, Vedado, Ciudad Habana, C.P. 10400, Cuba

We report exact diagonalization studies of inelastic light scattering in few-electron quantum dots under the strong confinement regime characteristic of self-assembled dots. We apply the orthodox (second-order) theory for scattering due to electronic excitations, leaving for the future the consideration of higher-order effects in the formalism (phonons, for example), which seem relevant in the theoretical description of available experiments. Our numerical results stress the dominance of monopole peaks in Raman spectra and the breakdown of selection rules in open-shell dots. The dependence of these spectra on the number of electrons in the dot and the incident photon energy is explicitly shown. Qualitative comparisons are made with recent experimental results.

PACS numbers: 78.30.-j, 73.21.La, 78.67.Hc

I. INTRODUCTION

Raman spectroscopy is a powerful tool in the investigation of the electronic properties of nanostructures¹. In a standard experiment, the energy of the incident light beam is slightly above the structure band gap (resonant conditions), and the scattered light is collected in the backward direction (backscattering geometry). Because of the fact that there are two photons involved in a Raman process, selection rules hold for the total angular momentum (or parity) of the electronic subsystem ($\Delta J = 0, \pm 2$). These selection rules are different from the rules governing intraband absorption ($\Delta J = \pm 1$, Kohn theorem), thus Raman spectroscopy allows us to study a different sector of the spectrum of electronic excitations in the dot.

In the last few years, Raman measurements in self-assembled quantum dots were reported^{2,3,4}. The distinctive features of these experiments are the observation of peaks, apparently violating the selection rules³, and the observation of a strong electron - LO phonon coupling (polaron effect⁵) in self-assembled dots⁴. The description of these effects requires a higher-order theoretical scheme⁶, in which parity-violating vertices are included, in addition to the two electron - photon vertices. We notice, however, that exact calculations for Raman scattering in few-electron quantum dots, even in the lowest (second) order scheme, are lacking. To the best of our knowledge, only a few calculations for etched dots are available^{7,8}, in which the final states are properly treated, but the intermediate states are not. We think that a precise understanding of the standard Raman scattering processes in few-electron quantum dots is needed as a basis towards the description of higher-order processes.

Thus, in the present paper we recall the orthodox

(standard) second-order Raman scheme for light scattering by electronic excitations in self-assembled quantum dots. We consider dots with up to six electrons. The needed wave functions to compute the Raman cross sections are obtained by exact diagonalization in a truncated basis set of many-particle functions. Because of the resonant character of the process, the intermediate states have an additional electron-hole pair. It means that the largest system we should diagonalize is made up from seven electrons and one hole. The strong confinement regime, characteristic of self-assembled dots, makes it possible to reach convergence in the numerical calculations with a relatively reduced basis set (of around 10^5 functions). We use the Lanczos algorithm in order to obtain the low-energy spectrum of our Hamiltonian.

The plan of the paper is as follows. In the next section, we present the model quantum dot and the way we compute the Raman transition amplitude. In section III, the intraband excitations of the quantum dot (the final states in a Raman process) are described. A criterium for the “collective” character of a many-particle state is given, which is based on the multipole operators appearing in the off-resonance asymptotics for the Raman amplitude⁹. In that section, we may appreciate how the collective and single-particle excitations shift in energy as the particle number or the confinement strength is varied. In addition, we appreciate how, for open-shell dots, states which are undoubtedly charge excitations give nonzero matrix elements of multipole “spin” operators. Next, in section IV the interband excitations are constructed. They are the intermediate states in a Raman event. We compute the interband absorption to get an idea of the position of the incoming resonances in Raman scattering. In section V, we present the Raman spectra. As it will be shown, the spectra are dominated by monopole peaks, both in

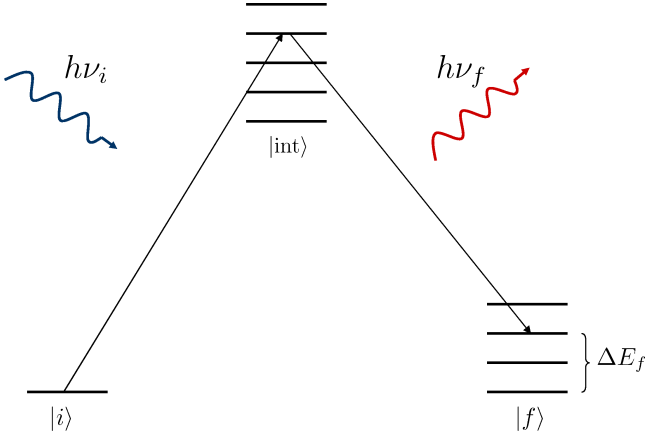


FIG. 1: (Color online) Schematic representation of an inelastic light scattering process.

polarized and depolarized geometries. This is in accord to the fact that the dot lateral dimensions (~ 20 nm) are shorter than $1/10$ of the light wavelength. Particularly interesting is the observed breakdown of the Raman selection rules in open-shell dots. Finally, in the last section, we qualitatively discuss the relevance of our calculations to the experiments detailed in Refs. [2,3,4].

II. THE FORMALISM

The values of the parameters used in our model for self-assembled quantum dots are motivated by the experiments in Refs. [2,3,4]. For the electron mass and dielectric constants we took, respectively, the following InAs values¹⁰: $m_e = 0.024 m_0$, and $\epsilon = 14.55 \epsilon_0$. The in-plane confinement potential is assumed parabolic, with a characteristic frequency $\hbar\omega_e$ ranging in the interval between 20 and 50 meV. This is, of course, a simplification. The actual confinement potential is expected to become flat already at excitation energies around 100 meV.^{3,4} We will study dots in which the number of electrons varies between 2 and 6.

Under resonance conditions, the Raman scattering transition amplitude is given by the following expression^{9,11,12,13}, coming from second order perturbation theory in the scattering matrix:

$$A_{fi} \sim \sum_{int} \frac{\langle f | H^{(+)} | int \rangle \langle int | H^{(-)} | i \rangle}{h\nu_i - (E_{int} - E_i) + i\Gamma_{int}}. \quad (1)$$

We schematically represent it in Fig. 1. $h\nu_i$ is the incident laser energy. The initial state in the process is the ground state of the N_e -electron system, meaning that we are considering a process at low temperatures, where only the ground state is populated and hence only Stokes lines in the Raman spectra should be observed. The final states in the process, on the other hand, are quantum dot

intraband excitations. Details on how the final states are computed, what their properties are, etc are given in the next section. We notice that conservation of energy leads to the following relation:

$$E_f - E_i = h\nu_i - h\nu_f, \quad (2)$$

allowing us to express the Raman shift (r.h.s. of Eq. (2)) in terms of the final state excitation energy. Varying $h\nu_i$, a peak at a fixed Raman shift (a resonance) indicates the existence of a final state (or group of states) with a given excitation energy. That is how Raman spectroscopy works.

Eq. (1) contains a sum over intermediate electronic states. The (virtual) transitions to the intermediate states are caused by the electron-photon interactions. Because of the denominator in Eq. (1), when $h\nu_i$ is slightly above the dot effective band gap the sum is dominated by the resonant terms, i.e. intermediate states with an additional electron-hole pair, whose energies are $E_{int} - E_i \approx h\nu_i$. They are described in section IV. The intermediate states play, of course, a role in A_{fi} . Incoming and outgoing resonances, i.e. increase in Raman intensities for precise values of $h\nu_i$ or $h\nu_f$, are a consequence of resonances with given intermediate states. However, the position of peaks in Raman spectra is determined solely by the final states. Notice that our expression, Eq. (1), differs from that one used in Refs. [7,8] precisely in the treatment of the intermediate states, which we consider as many-particle and Coulomb interacting states. This allows us to correctly describe incoming and outgoing resonances in Raman scattering.

The electron-photon vertices entering Eq. (1), $H^{(-)}$ and $H^{(+)}$, are single-particle operators in which matrix elements over photon operators were explicitly computed. The - and + supraindexes refer to absorption or emission of a photon, respectively. $H^{(-)}$, for example, is given by:

$$H^{(-)} = \sum_{\sigma\tau} \langle \sigma | e^{i\vec{q}_i \cdot \vec{r}} \vec{\epsilon}_i \cdot \vec{p} | \bar{\tau} \rangle e_{\sigma}^{\dagger} h_{\tau}^{\dagger}, \quad (3)$$

where we use a basis of two-dimensional oscillator states, σ and τ , for electrons and holes¹⁴. \vec{q}_i and $\vec{\epsilon}_i$ are the wave vector and polarization of the incident photon. Notice that the electron state in the valence band, $\bar{\tau}$ (conjugate of the hole state τ), enters the matrix element in $H^{(-)}$.

For $H^{(+)}$, we use the relation:

$$\langle f | H^{(+)} | int \rangle = \langle int | H^{(-)} | f \rangle^* \Big|_{\vec{q}_f, \vec{\epsilon}_f}, \quad (4)$$

where the matrix element in the r.h.s. is to be evaluated with the wave vector and polarization of the scattered photon.

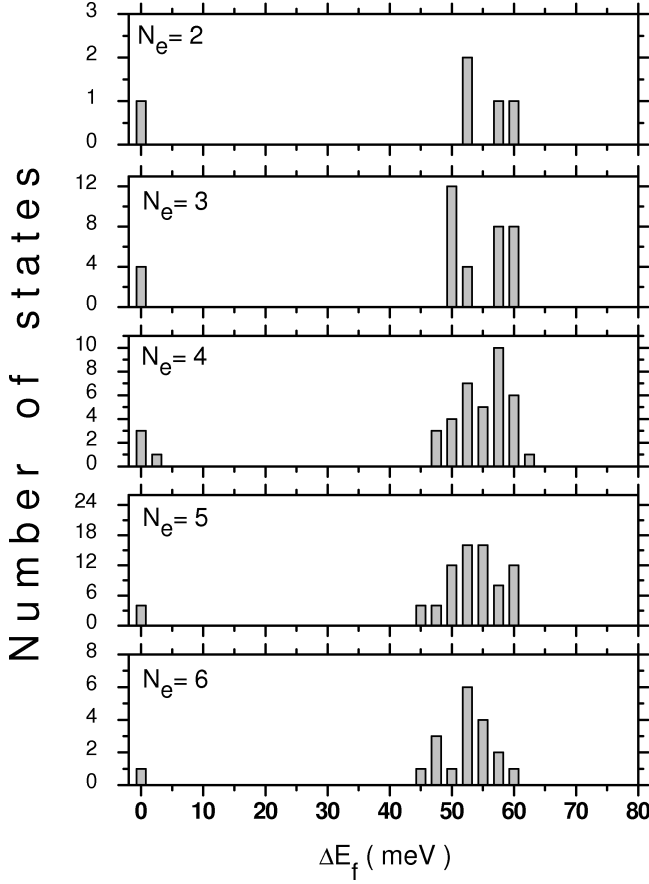


FIG. 2: Density of energy levels in few-electron dots for $\hbar\omega_e = 30$ meV and excitation energy below 100 meV. See explanation in the text.

III. INTRABAND EXCITATIONS IN SELF-ASSEMBLED DOTS

Self-assembled InAs dots take usually the form of disks, of around 20 nm diameter and 5 nm high¹⁵. We assume that the motion of electrons along the axis (z -direction) is quantized, occupying the first sub-band. For the motion in the perpendicular plane, we use a harmonic oscillator model.

In order to compute the intraband excitations of the N_e -electron quantum dot we diagonalize the electronic Hamiltonian

$$H = \sum_{\sigma} (E_z^{(e)} + \hbar\omega_e \varepsilon_{\sigma}) e_{\sigma}^{\dagger} e_{\sigma} + \frac{\beta}{2} \sum_{\lambda\mu\sigma\tau} \langle \lambda, \mu | \frac{1}{r_{12}} | \sigma, \tau \rangle e_{\lambda}^{\dagger} e_{\mu}^{\dagger} e_{\tau} e_{\sigma}, \quad (5)$$

in a basis of Slater determinants. In Eq. (5), $E_z^{(e)} = \hbar^2 \pi^2 / (2m_e L_z^2)$, and $L_z = 5$ nm is the dot width. The energy of 2D oscillator states is $\varepsilon_{\sigma} = 2k_{\sigma} + |l_{\sigma}| + 1$, where k is the radial quantum number, and l is the angular mo-

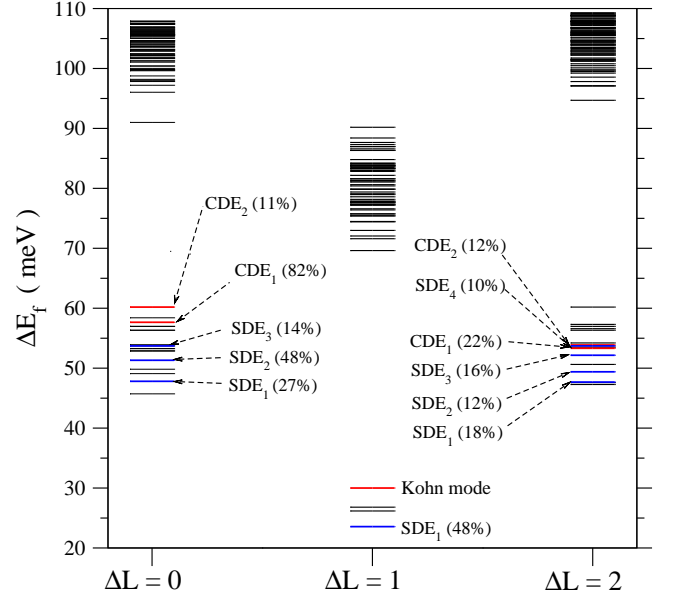


FIG. 3: (Color online) The low-lying intraband excitations in the 6-electron quantum dot. $\hbar\omega_e = 30$ meV. The relative contribution to energy-weighted sum rules of collective states is given.

mentum along the normal to the plane. The matrix elements of Coulomb interactions, $\langle \lambda, \mu | 1/r_{12} | \sigma, \tau \rangle$, among any four states of the first 20 oscillator shells were computed and stored in a file. The strength of Coulomb interactions is given by $\beta = e^2 / (4\pi\epsilon l_e)$, where e is the electron charge, and l_e the electron oscillator length. With the explicit values of the parameters, we get $\beta = 1.75 \sqrt{\hbar\omega_e}$ meV, where $\hbar\omega_e$ is to be written in meV also. Notice that the ratio between characteristic Coulomb and oscillator energies, $\beta/\hbar\omega_e$, is less than one for self-assembled dots (around 0.25 for $\hbar\omega_e = 50$ meV).

The dimension of the Hamiltonian matrix can be reduced by restricting the basis to sectors with given values of the total angular momentum, $L = \sum_{\sigma} l_{\sigma}$, and total spin projection, $S_z = \sum_{\sigma} s_z \sigma$. The dimension is further reduced by introducing an energy cutoff. Due to the strong confinement, we obtain converged eigenvalues of the Hamiltonian (5) using a truncated basis of Slater determinants with zeroth-order (harmonic oscillator) excitation energy lower than $8 \hbar\omega_e$. This leads to matrices with dimensions less than 10^4 which are easily diagonalized. The algorithm used in our Fortran 90 code has many similarities with published ones^{16,17,18}. It is not yet parallelized, although it may be easily adapted for parallel computation.

A sample of the results is shown in Fig. 2 for dots with $N_e = 2 - 6$, and $\hbar\omega_e = 30$ meV. In this figure, we present the density of energy levels for the excited states with the same L and S_z as the ground states. These are the final states giving the main contribution to the Raman cross section. Notice the ground-state degeneracies in the

$N_e = 3$ dot (quantum numbers: $L = \pm 1$, $S_z = \pm 1/2$), in the $N_e = 4$ dot ($L = 0$, $S_z = 0, \pm 1$), and in the $N_e = 5$ dot ($L = \pm 1$, $S_z = \pm 1/2$).

A more detailed view of the spectrum of excited states in the 6-electron dot is drawn in Fig. 3. This is a closed-shell system with ground-state quantum numbers $L_i = S_i = 0$. Using a common terminology¹², we will refer to $\Delta L = L_f - L_i = 0$ states as monopole excitations, $\Delta L = \pm 1$ states as dipole excitations, $\Delta L = \pm 2$ states as quadrupole excitations, etc. On the other hand, states with total spin variation, $\Delta S \neq 0$, will be called spin excitations, even if $\Delta S_z = 0$, in contrast to charge excitations which correspond to $\Delta S = 0$. The cases $\Delta S_z \neq 0$ (spin flips) will not be considered below because the Raman amplitudes for transitions to such states are very small^{12,13}. Spin-flip peaks in the Raman spectra are the result of higher-order processes and will not be studied in the present paper.

In Fig. 3, collective states are also indicated. By collective we mean many-particle states of interacting electrons with significant matrix elements of multipole operators. Let us recall the energy-weighted sum rule for charge excitations¹⁹:

$$\sum_f \Delta E_f \{ |\langle f | D_{\Delta L}^{(c)} | i \rangle|^2 + |\langle f | D_{\Delta L}^{(c)\dagger} | i \rangle|^2 \} = \langle i | [D_{\Delta L}^{(c)}, [H, D_{\Delta L}^{(c)\dagger}]] | i \rangle. \quad (6)$$

A state $|f\rangle$ will be conventionally called collective (a charge-density excitation, CDE) if $\Delta E_f |\langle f | D_{\Delta L}^{(c)} | i \rangle|^2$ is greater than 5% of the r.h.s. of Eq. (6). In contrast, a state with a small contribution to the sum rule is called a single-particle excitation (SPE). The multipole operator is defined as:

$$D_{\Delta L}^{(c)} = \sum_{\lambda, \mu} \langle \lambda | d_{\Delta L} | \mu \rangle e_{\lambda}^{\dagger} e_{\mu}, \quad (7)$$

where the sum runs over states λ and μ with the same spin projection. The matrix elements $\langle \lambda | d_{\Delta L} | \mu \rangle$ are given elsewhere^{13,20}. Making explicit the spin degrees of freedom, we write:

$$D_{\Delta L}^{(c)} = \sum_{\lambda, \mu} \langle \lambda | d_{\Delta L} | \mu \rangle (e_{\lambda\uparrow}^{\dagger} e_{\mu\uparrow} + e_{\lambda\downarrow}^{\dagger} e_{\mu\downarrow}), \quad (8)$$

in which λ and μ now refer to orbital functions (no spin). These operators $D_{\Delta L}^{(c)}$ enter the asymptotic expression for the Raman amplitude in the off-resonance regime⁹. They are multiplied by the scalar product, $\vec{\epsilon}_i \cdot \vec{\epsilon}_f$, between the incident and scattered light polarization vectors.

On the other hand, a second term in the asymptotic off-resonance expression⁹, proportional to $(\vec{\epsilon}_i \times \vec{\epsilon}_f) \cdot \hat{z}$, involves the operator

$$D_{\Delta L}^{(s)} = \sum_{\lambda, \mu} \langle \lambda | d_{\Delta L} | \mu \rangle (e_{\lambda\uparrow}^{\dagger} e_{\mu\uparrow} - e_{\lambda\downarrow}^{\dagger} e_{\mu\downarrow}). \quad (9)$$

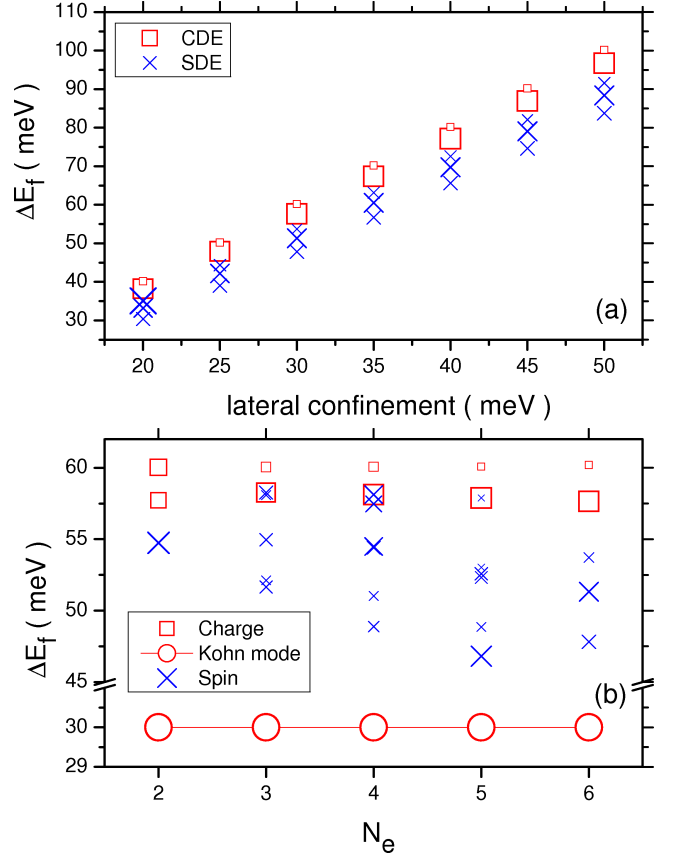


FIG. 4: (Color online) (a) Collective monopole excitations below 100 meV in the six-electron dot as a function of $\hbar\omega_e$. (b) Sum rule fractions for monopole states in the few-electron dots and a confinement potential with $\hbar\omega_e = 30$ meV. The Kohn mode (dipole excitation) is also drawn as a reference.

This operator may serve to distinguish collective spin excitations (spin density excitations, SDE) only when the ground-state total spin is $S_i = 0$. When $S_i \neq 0$, the correspondence is not unique, meaning that we could observe peaks corresponding to charge excitations in the cross-polarized Raman spectrum of open-shell dots.

Notice that, in Fig. 3, the dipolar SDE's are the lowest states in that sector, and the monopole CDE's are at the top of the first group of monopole states, having excitation energies roughly equal to $2 \hbar\omega_e$.

Fig. 4(a) shows the collective states of the six-electron dot as a function of the confinement strength, $\hbar\omega_e$. States have been denoted by symbols, whose sizes are proportional to their weight in the corresponding sum rule.

On the other hand, in the lower panel of Fig. 4, the harmonic energy is fixed at $\hbar\omega_e = 30$ meV, and the monopole states with fractions of the charge or spin sum rules higher than 5% are drawn as a function of the number of electrons in the dot. There is, in addition, a remarkable fact in these dots, working under the strong-confinement regime, related to the position of the main CDE state: it is almost independent of the number of

$N_e = 2, L = 0, S = 0$	ΔE_f (meV)	$S_1^{(c)}$	$S_1^{(s)}$	ΔS
SDE ₁	54.74	0 %	96 %	+1
CDE ₁	57.72	43 %	0 %	0
CDE ₂	60.03	51 %	0 %	0
$N_e = 3, L = \pm 1, S = 1/2$	ΔE_f (meV)	$S_1^{(c)}$	$S_1^{(s)}$	ΔS
SDE ₁	51.65	0 %	21 %	+1
SDE ₂	52.11	0 %	10 %	+1
CE ₁	54.96	0 %	22 %	0
CE ₂	58.08	0 %	11 %	0
CDE ₁	58.27	69 %	23 %	0
CDE ₂	60.05	26 %	0 %	0
$N_e = 4, L = 0, S_z = \pm 1$	ΔE_f (meV)	$S_1^{(c)}$	$S_1^{(s)}$	ΔS
SDE ₁	48.88	0 %	16 %	+1
CE ₁	51.02	0 %	11 %	0
CE ₂	54.41	0 %	22 %	0
CDE ₁	58.13	80 %	41 %	0
CDE ₂	60.07	18 %	5 %	0
$N_e = 4, L = 0, S_z = 0$	ΔE_f (meV)	$S_1^{(c)}$	$S_1^{(s)}$	ΔS
SDE ₁	48.88	0 %	20 %	+1
SDE ₂	54.48	0 %	41 %	-1
SDE ₃	57.47	0 %	33 %	-1
$N_e = 5, L = \pm 1, S = 1/2$	ΔE_f (meV)	$S_1^{(c)}$	$S_1^{(s)}$	ΔS
SDE ₁	46.80	0 %	6 %	+1
SDE ₂	48.86	0 %	12 %	+1
SDE ₃	52.31	0 %	20 %	+1
CE ₁	52.58	0 %	23 %	0
SDE ₄	53.03	0 %	7 %	+1
CDE ₁	57.88	84 %	6 %	0
CDE ₂	60.08	11 %	0 %	0
$N_e = 6, L = 0, S = 0$	ΔE_f (meV)	$S_1^{(c)}$	$S_1^{(s)}$	ΔS
SDE ₁	47.81	0 %	27 %	+1
SDE ₂	51.31	0 %	48 %	+1
SDE ₃	53.72	0 %	14 %	+1
CDE ₁	57.65	82 %	0 %	0
CDE ₂	60.19	11 %	0 %	0

TABLE I: The sum rule fractions represented in Fig. 4(b). $S_1^{(c,s)}$ refer, respectively, to the charge and spin energy-weighted sum-rule fractions. Charge-excitation states giving only contributions to the spin sum rule are denoted CE's.

electrons in the dot. Explicit values of the sum rule fractions are given in Table I. Notice that, in the open-shell dots, charge excitations (collective or not) may also give a contribution to the “spin” sum rule.

IV. THE INTERBAND EXCITATIONS

The intermediate states entering Eq. (1) for the transition amplitude are interband excitations of the dot, i.e. states with an additional electron-hole pair. We will use a simplified description with only one (heavy) hole band with effective anisotropic mass, $m_h^{(z)} = 0.35 m_0$, $m_h^{(xy)} = 0.035 m_0$.¹⁰ This is not a very crude hypothesis, which may be justified to work in the conditions of self-assembled dots because of the shift of light-hole states due to the small width of the dots along the symmetry

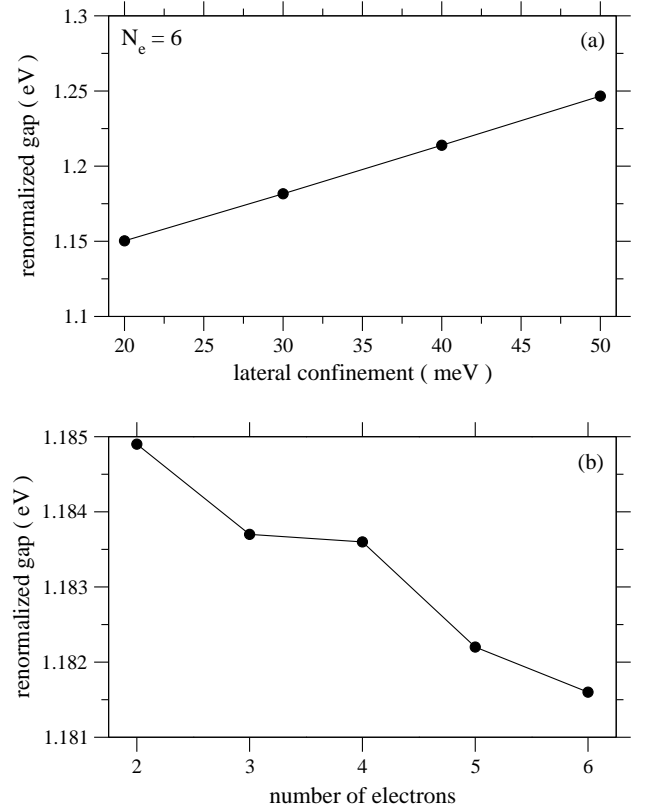


FIG. 5: (a) The effective band gap in the six-electron dot as a function of $\hbar\omega_e$. (b) Band gap in the few-electron dots for a confinement potential with $\hbar\omega_e = 30$ meV.

axis. Indeed, when $L_z = 5$ nm, light hole states are 0.5 eV higher in energy than heavy hole states.

Under this simplification, the intermediate states are characterized by the total angular momentum, L_{int} , the hole spin projection, $S_z^{(h)}$, and the total electronic spin projection, $S_z^{(e)}$. The main contribution to the Raman amplitude comes from states in which the added pair has angular momentum equal to zero, that is $L_{int} = L_i$, where L_i is the initial (ground) state angular momentum of the N_e -electron system.

We should then diagonalize the Hamiltonian (5) with two additional terms

$$\sum_{\sigma} (E_z^{(h)} + \hbar\omega_h \varepsilon_{\sigma}) h_{\sigma}^{\dagger} h_{\sigma} - \beta \sum_{\lambda\mu\sigma\tau} \langle \lambda, \mu | \frac{1}{r_{12}} | \sigma, \tau \rangle e_{\lambda}^{\dagger} h_{\mu}^{\dagger} h_{\tau} e_{\sigma}, \quad (10)$$

the first one represents the single-particle energy of the hole, and the second one accounts for the electron-hole interactions. The basis functions are built up as products of Slater determinants for electrons and a single harmonic-oscillator function for the hole. As in the previous section, we define the excitation energy for these functions in terms of the difference of zero-order (harmonic-oscillator) energies. The reference is the lowest energy in the basis.

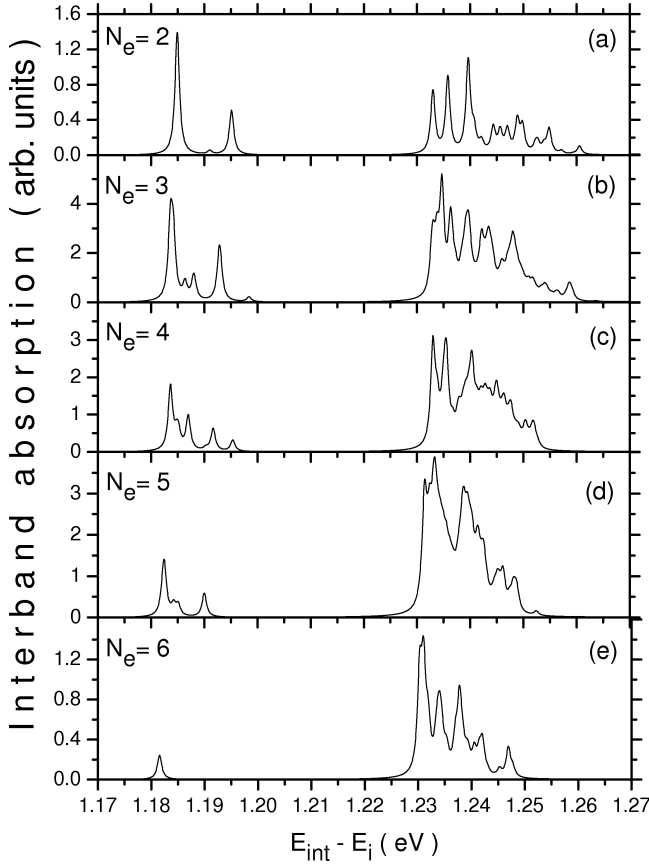


FIG. 6: Interband absorption in the few-electron dots with a confinement potential $\hbar\omega_e = 30$ meV. The spectra were calculated assuming a uniform width $\Gamma_{int} = 0.5$ meV for the intermediate states.

With a cutoff of $8 \hbar\omega_e$ for the excitation energy (enough to reach convergence), matrix dimensions of around 10^5 are obtained. The lowest 100 eigenvalues are easily computed by means of Lanczos algorithms²¹.

We show in Fig. 5 the gap renormalization effects in the dots as a result of varying the confinement strength or the number of electrons. The renormalized gap is simply the energy difference between the lowest intermediate state and the ground state in the dot. Notice that the effective gap (around 1.18 eV) is the result of adding a nominal $E_{gap} = 0.43$ eV, the confinement energies along the z -direction of the added electron and hole ($E_z^{(e)} + E_z^{(h)}$), the in-plane confinement energies of both particles, and the contribution from Coulomb interactions. The dependence on $\hbar\omega_e$ is almost linear, as expected, because of the single-particle terms in the Hamiltonian. The small redshift of the effective band gap with increasing N_e , on the other hand, comes from the prevalence of electron-hole attractive interactions over phase-space filling effects in small dots.

In Fig. 6, we show the interband absorption in dots with $N_e = 2, \dots, 6$ and $\hbar\omega_e = 30$ meV. The intention is to show possible incoming resonances in Raman scat-

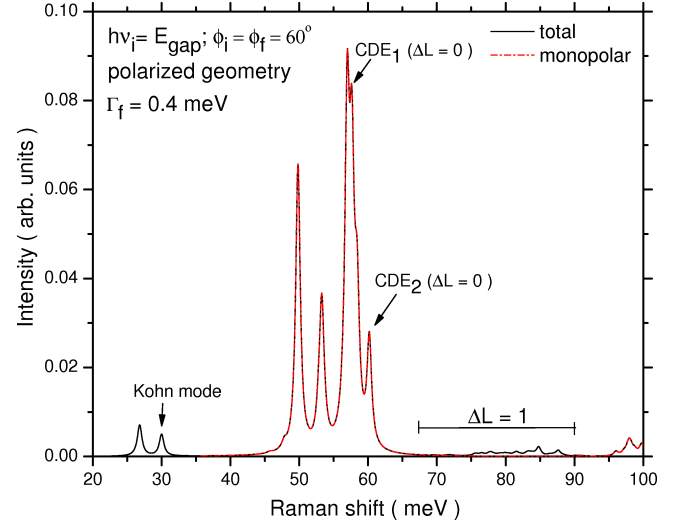


FIG. 7: (Color online) Polarized Raman spectrum for a six-electron dot with confinement $\hbar\omega_e = 30$ meV. Monopolar (dashed line) and total (solid line) spectra are drawn. The total cross-section includes contributions from monopole, dipole, and quadrupole states.

tering processes. The absorption spectrum at normal incidence is computed from the matrix elements squared, $|\langle int | H^{(-)} | i \rangle|^2$, smeared out with a Lorentzian. We used a uniform width for the intermediate states, $\Gamma_{int} = 0.5$ meV. Only intermediate states with the same angular momentum as the electronic ground states are included in the computation, that is $L_{int} = L_i$. Two spin combinations are considered $S_{z,int}^{(e)} = S_{z,i}^{(e)} + 1/2$, $S_{z,int}^{(h)} = -1/2$, and $S_{z,int}^{(e)} = S_{z,i}^{(e)} - 1/2$, $S_{z,int}^{(h)} = 1/2$.

Although $\hbar\omega_e = 30$ meV is not the strongest confinement achievable in self-assembled dots, we clearly distinguish in Fig. 6 absorption peaks arranged in shells separated by $2\hbar\omega_e$. The dispersion of peaks in the first shell ranges from 15 meV in the $N_e = 2$ dot to a single (doubly degenerate) peak in the 6-electron dot. Incoming resonances in a Raman spectra should be then very sharp if experiments were conducted in a very high quality dot array or a single dot with the use of confocal microscopy.

Specially interesting is the 6-electron dot, where an almost ideal Raman process with transitions through a single intermediate resonance at 1181.6 meV can be realized.

Results for Raman cross-sections are presented in the next section.

V. RAMAN SPECTRA

The first feature of Raman spectra in self-assembled dots is the dominance of monopole ($\Delta L = 0$) peaks. This property is shared with etched dots^{12,22}, but it is much more accentuated for self-assembled dots because of their

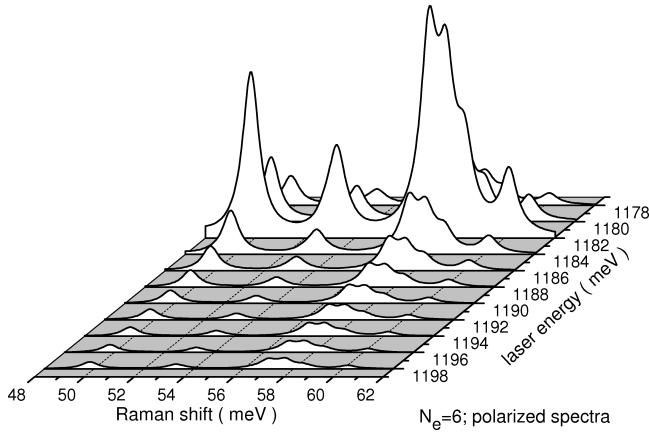


FIG. 8: Polarized Raman spectrum in the six-electron dot as a function of the incident laser energy.

smaller dimensions. Indeed, the typical diameter, d , of InAs dots in a GaAs matrix, for example, is around 20 nm. On the other hand, the Raman amplitude squared, $|A_{fi}|^2$ for a state $|f\rangle$ with a given ΔL is proportional to $(q_i \sin \phi_i d)^{2|\Delta L|}$, where ϕ_i is the angle of incidence of photons, and $q_i \approx 0.006 \text{ nm}^{-1}$ is the wavevector of photons with energy equal to 1.18 eV. The product $q_i d$ is roughly 0.12, meaning that only $\Delta L = 0$ peaks should be observed.

We show in Fig. 7 the spectrum for a $N_e = 6$ dot and $\hbar\omega_e = 30 \text{ meV}$. The incident photon energy is exactly in resonance with the first exciton state shown in Fig. 6 (e), that is $\hbar\nu_i = 1181.6 \text{ meV}$. The differential cross-section is computed from the expression:

$$d\sigma \sim \sum_f |A_{fi}|^2 \frac{\Gamma_f/(4\pi)}{\Gamma_f^2 + (\hbar\nu_f + E_f - E_i - \hbar\nu_i)^2}, \quad (11)$$

where we used a Lorentzian to smear out the Dirac delta function expressing conservation of energy, Eq. (2). The width of final states, Γ_f , is assumed uniform and equal to 0.4 meV. When the ground state is degenerate, we sum over all of the terms in the multiplet.

The calculations shown in Fig. 7 correspond to the polarized geometry, under backscattering conditions and incidence angle (in vacuum) equal to 60° in order to strengthen multipole peaks. Contributions from $\Delta L = 0$ (monopole), $\Delta L = \pm 1$ (dipole), and $\Delta L = \pm 2$ (quadrupole) final state excitations are included in the sum in Eq. (11). Dipole final states with Raman shifts around 30 meV (in particular, the Kohn mode) and around 80 meV give rise to peaks at least one order of magnitude smaller than the leading monopole peaks lying in the interval from 50 to 60 meV. Quadrupole states, present also in this interval (see Fig. 3), give, however, a negligible contribution to the cross-section. Notice that, under resonance conditions, peaks associated with single-particle monopole excitations are as strong as the

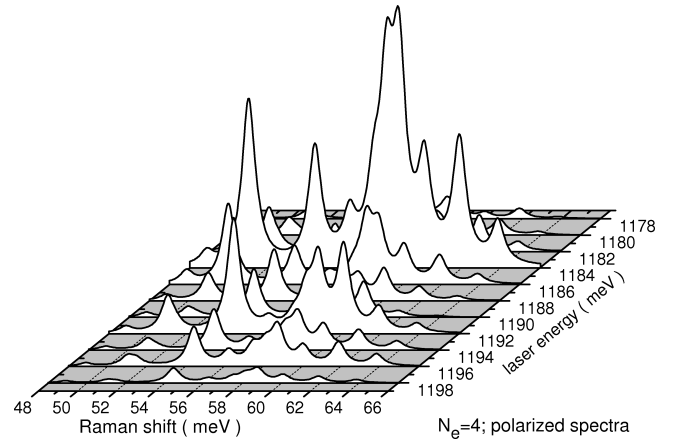


FIG. 9: Polarized Raman spectrum for a four-electron dot with confinement $\hbar\omega_e = 30 \text{ meV}$. The initial photon energy is varied in the interval where the first set of incoming resonances is expected.

peaks corresponding to the collective states (CDE). Let us stress also that the main Raman peaks are shifted 50 - 60 meV below the luminescence lines and, for this reason, should be easily observable.

Polarized spectra for the six-electron dot as a function of the incident photon energy, $\hbar\nu_i$, are shown in Fig. 8. The incident angle in this and the next figures is $\phi_i = 10^\circ$. Due to the special character of these processes, with transitions through a single intermediate state resonance, the dependence on $\hbar\nu_i$ is uniform, with a sharp maximum at the resonance. Away from the resonance, on both sides of it, the CDE₁ state gives the strongest peak.

The $N_e = 6$ spectra may be contrasted with the $N_e = 4$ polarized spectra, shown in Fig. 9. The $\hbar\nu_i$ intervals shown in both figures are the same in order to facilitate comparison. Resonances with different intermediate states (see Fig. 6) lead, in the present case, to a pattern in which the relative intensities of Raman peaks rapidly vary with $\hbar\nu_i$. This is the common feature of all of the studied dots except the $N_e = 6$ one. There are also interesting facts about the Raman spin selection rules, but they are more evident in the next Fig. 10, where polarized and depolarized spectra are drawn as a function of N_e .

Monopolar spectra in Fig. 10 are computed at incident photon energy exactly in resonance with E_{gap} of each dot. First, we notice that for the $N_e = 2$ and $N_e = 6$ (closed-shell) dots, in which the ground-state total electronic spin is $S_i = 0$, the spin selection rules deduced in the off-resonance regime (ORA) hold even under resonance conditions²³. That is, CDE's and SPE's with $\Delta S = 0$ are observed in the polarized spectrum, and SDE's and SPE's with $\Delta S = 1$ are observed in the depolarized spectrum. This is not the case for the open-shell dots, in particular the $N_e = 3$ and 5 dots, for which the polarized and depolarized spectra are very similar, and we can not use the selection rules in order to identify spin

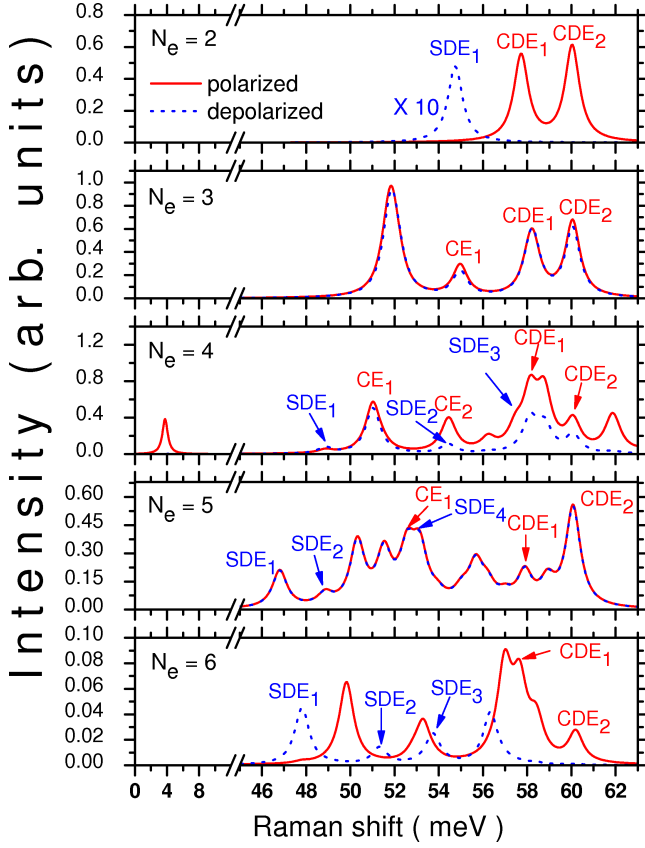


FIG. 10: (Color online) Polarized and depolarized monopolar Raman spectra in the few-electron dots with confinement $\hbar\omega_e = 30$ meV. The initial photon energy is exactly in resonance with the first intermediate state (E_{gap}) in each dot.

or charge excitations. In the $N_e = 4$ dot, we observe the singlet state (a spin excitation), which can be classified as a SPE according to the sum rule, as a distinct low-energy peak in the polarized spectrum. Notice that, in general, the weights in the sum rule given in Table I are not indicative of the relative intensities of peaks in the Raman spectrum. On the other hand, the positions of CDE's states practically do not depend on N_e , specially the CDE_2 , as mentioned in the comments to Fig. 4, and the SDE's peaks shift to lower energies as N_e is increased.

Finally, we would like to address the question about outgoing resonances. These resonances are defined by following the intensity of a fixed Raman peak as a function of the energy of the scattered photon. In bulk systems, outgoing resonances associated with collective final states were found at exactly the same energy positions of incoming resonances, which led to the idea that outgoing resonances are a consequence of a third-order process, in which an additional perturbation causes the decay of the intermediate state towards the exciton (incoming resonance).²⁴ We would like to check what happens when employing exact functions in the standard (second-order) scheme.

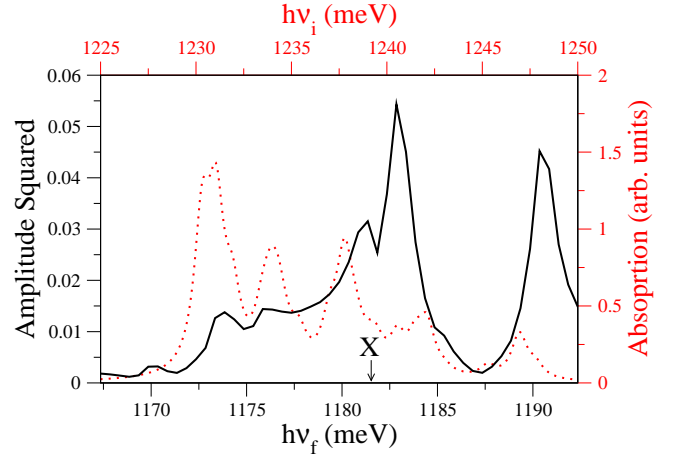


FIG. 11: (Color online) The amplitude squared, $|A_{fi}|^2$, solid line, corresponding to the CDE_1 state in the $N_e = 6$ dot and $\hbar\omega_e = 30$ meV as a function of the scattered photon energy, $h\nu_f$. The absorption intensity (dashed line) is also shown for comparison. Notice that the x axis in the absorption curve corresponds to $h\nu_i$. The energy of the first incoming resonance is indicated by an arrow.

Fig. 11 shows the amplitude squared, $|A_{fi}|^2$, corresponding to the CDE_1 state, that is, the most collective charge-density state, in the $N_e = 6$ dot and $\hbar\omega_e = 30$ meV, as a function of the scattered photon energy, $h\nu_f$. A strong peak at $h\nu_f \approx 1183$ meV, 1.4 meV above the energy of the first incoming resonance (indicated by an arrow in the figure), is observed. In our scheme, this means a strong resonance with an intermediate state with energy $E_{int} \approx E_X + \Delta E(CDE_1)$, where $E_X = 1181.6$ meV is the position of the first absorption maximum (exciton), and $\Delta E(CDE_1) = E_f(CDE_1) - E_i$. Comparison with the absorption intensity, also depicted in the figure with a dashed line, shows that the absorption peak is not the strongest for this particular intermediate state. This means that the matrix element corresponding to virtual emission of a photon, $\langle f|H^{(+)}|int\rangle$, should be particularly strong for this intermediate state, see Eq. (1). We verified a similar situation with regard to the most collective spin-density excitation (the SDE_2). The existence of an intermediate state with such characteristics, energy approximately equal to the sum of two eigenenergies, and a strong transition probability to the collective state, suggest a kind of approximate dynamical symmetry, and requires further research.

VI. QUALITATIVE ANALYSIS OF REPORTED EXPERIMENTS

Although there have been a number of reports of experimental Raman studies dating from the 1990s of deep-etched quantum dots with large numbers (hundreds) of electrons (see, for example, Refs. 25,26,27), apart

from two preliminary theoretical studies for 6 and 12 electrons^{28,29}, the initial experimental investigations of inelastic light scattering from quantum dots containing few electrons commenced in 2000. In that year Chu et al.² observed at 5 K under resonance excitation from self-assembled InGaAs/GaAs quantum dots a Raman peak near 50 meV with a linewidth of about 25 meV. Similar Raman spectra were observed in both polarized and depolarized scattering conditions without any apparent depolarization shift. From sample doping considerations and other experiments, Chu et al. deduced that there were about six electrons in each quantum dot and that the ground and first excited state of the dot were occupied. They interpreted the depolarized Raman peak as arising from SDEs while the polarized peak was associated with charge density fluctuations. Our calculations can help clarify this assignment. As mentioned in Section V and shown in Fig. 7, monopole Raman scattering dominates in few electron dots at resonance and the Raman spectrum of a closed shell dot containing six electrons should exhibit a clear difference between SDEs in the depolarized scattering geometry and CDEs in polarized scattering. This was not the case in Chu et al.'s work. On the other hand, for five, but not four, electrons confined in the dot, the polarized and depolarized spectra are expected to be very similar. Thus the broad 50 meV peak observed by Chu et al., which covers the right energy range according to our theory for a confinement energy of 30 meV, is definitely electronic in origin, is due to intersublevel transitions within the conduction band, and is well explained by taking five instead of six electrons in their dots. The lack of the expected fine structure, as shown in Fig. 10, in their reported spectrum is, as they also note, probably due to energy level variations in the conduction band arising from a statistical distribution of dot diameters in their sample.

In 2003, Brocke et al.³ investigated the electronic excitations in InGaAs/GaAs self assembled quantum dots where the dots could be filled with from 1 to 6 electrons by varying a gate voltage across the dots. Their resonant Raman scattering experiments revealed a broad Raman band in the energy range 40-55 meV in the polarized geometry (there was not mention of the depolarized spectrum in this paper). A feature of their results was the prominent peak observed at ~ 50 meV (linewidth of ~ 5 meV) for two electrons in the dots that was assigned to a CDE. This peak was seen to gradually shift to lower energy (~ 46 meV for six electrons) with increasing number of electrons in the dots. The shift was opposite in direction to their expectations for CDEs and was explained in terms of the Coulomb interaction amongst the dot electrons. Apart from the Kohn mode at 50 meV, their energy level calculations showed the existence of other excitations to lower energy (in the range 40-50 meV) for greater than two electrons per dot, but these additional low energy excitations were not individually resolved in the experiments³. No calculated Raman spectra were given in this paper. Without this information, the im-

plication of their energy level analysis performed using a confinement energy of 50 meV is that the clear peak they observed at ~ 50 meV for at least 2 electrons per dot was the Kohn mode. Our calculations of the Raman spectrum although for pure InAs dots with a confinement energy of 30 meV produce Raman peaks in a similar energy range to that observed by Brocke et al., and most importantly show that the $\Delta L = 1$ transitions including the Kohn mode at 30 meV give negligible contributions to the Raman intensity under resonance excitation. The present calculations show that in polarized scattering two CDEs spaced by 2-3 meV (CDE₁ and CDE₂ shown in Fig. 10) are prominent, but their energies do not shift much with increasing number of electrons in the dot (see Fig. 4). Based on these results, we can reinterpret the Raman results of Brocke et al. as follows. Their spectra show a peak at ~ 45 meV and evidence that a similar peak occurs at ~ 50 meV (this peak is more clearly seen at low and high electron numbers) that do not shift with electron number and are thus likely due to CDEs. The apparent shift of the ~ 50 meV peak to lower energy with increasing electron number is an illusion created by the appearance of additional Raman peaks at energies between 45 and 50 meV, especially for 4 and 5 electrons (see Fig. 10), that are unresolved in the Brocke et al. experiments. A more quantitative analysis than this requires further detailed calculations for the specific physical properties of their dot structure.

More recently, resonance Raman scattering experiments have been performed on InAs/GaAs self-assembled quantum dots filled by n-type modulation doping with 5, 7, and 12 electrons⁴. Detailed results were published for ~ 7 electron dots with intersublevel transitions in the ~ 50 meV range. On resonance excitation a broad electronic Raman line was observed at 57 meV (linewidth ~ 15 meV) in a near-polarized geometry that was attributed to intersublevel electron transitions. No detailed structure of this Raman band was noted for ~ 7 electrons,⁴ but its peak energy increased slightly with increasing number of dot electrons from 55 meV for ~ 5 electrons to 63 meV for ~ 12 electrons, at which point some band structure became evident.³⁰ As opposed to the Brocke et al. results,³ the apparent peak position of this Raman band increases slightly with the number of electrons per dot and thus is in accord with an assignment to CDEs. Although our calculations for InAs quantum dots extend only to 6 electrons they show that there are two CDEs expected in the vicinity of the 57 meV peak observed by Aslan et al. and they do not shift much in energy with increasing number of electrons. In fact, the calculated polarized monopolar Raman spectrum shown in Fig. 10 for 6 electrons exhibits a maximum at 57 meV and, when appropriately broadened, resembles quite well the experimentally observed Raman band for ~ 7 electrons. One additional interesting aspect of the work of Aslan et al. was their observation of strong coupling between quantum dot longitudinal-optical phonons and electron intersublevel transitions.⁴ Such coupling modifies the signatures

of both the phonon and electronic Raman lines and thus for better comparison with experiment further theoretical calculations including the effects of electron-phonon coupling are desirable. Once such theoretical results are obtained, it will become clear as to whether or not the broad Raman electronic lines in these samples are intrinsic or, more likely, due to dot structural inhomogeneities, as discussed above.

In 2005, Garcia et al.⁷ reported on the low energy electronic excitations in AlGaAs/GaAs etched quantum dots where the dots were filled with a distribution of from 4 to 6 electrons by modulation doping. The confinement energy was small for their sample (4 meV) and they observed electronic excitations in the energy range 4-10 meV. On taking into account the difference in confinement energies between their value and ours of 30 meV (giving a $7.5\times$ energy level scaling factor, approximately), however, a qualitative comparison with our theoretical results is still possible. Allowing for the breadth (linewidths of ~ 2 -3 meV) of the two main peaks seen in the polarized and also the depolarized geometries, as also reported in subsequent work from the same group,³¹ their results are consistent with a weighted summation in the two geometries of our calculated spectrum for 4, 5 and 6 electrons giving two lower energy SDEs along with a nearby CDE together with a number of similar (unresolved experimentally) excitations to higher energy. A somewhat sharper peak than the other CDEs and SDEs was observed at 5.5 meV in the depolarized geometry by Garcia et al. and it was attributed by them to an inter-shell monopole spin mode with $\Delta S = -1$. Such a transition is a special characteristic of dots containing four electrons only. Our calculations not only confirm this mode assignment (SDE2) but also reveal a second $\Delta S = -1$ mode at higher energy (SDE3), as can be seen in Table I; these are precisely the monopole singlet ($S = 0$) states in the $N = 4$ dot. In our strong-confinement regime, the calculated SDE Raman peaks are not as prominent as, but have similar widths to, the main CDE Raman peaks (see Fig. 10). However, in the weak-confinement regime of Garcia et al., the SDE peaks could become stronger, because of the increasing role played by Coulomb interactions in that regime. Dot-ensemble induced inhomogeneous broadening likely precluded Garcia et al. from observing the higher energy and weaker SDE3 Raman peak.

In summary, our theoretical results have proved to be in qualitative agreement with experiment. However, in general, not all the detailed structure predicted in our calculations and its polarization dependence for dots filled with from 2 to 6 electrons has been observed experimentally, because of the wide widths (typically in the range 5-25 meV for InGaAs/GaAs dots) of the Raman bands. This is partly due to present samples comprising dots filled with a range of electrons and also to variations in the size of dots in a given sample. Thus for a better comparison between theory and experiment there is now a need for more experimental work on better defined arrays

of dots or, better still, on single dots. Finally, we consider the obverse case of resonant Raman scattering from holes in self assembled dots. Such scattering has been only rarely investigated to date, but has been observed in both SiGe/Si³² and InAs/GaAs³³ quantum dots. In the latter work on InAs dots, p-type doping resulted in 2-5 holes per dot depending on the as-grown dot density. Resonant Raman scattering from such samples produced a broad intersublevel hole excitation at ~ 25 meV (linewidth ~ 12 meV) for 2-3 holes per dot that shifted to lower energies with increasing numbers of holes per dot. The small difference in the valence intraband energy values obtained by Raman and photoluminescence spectra was explained qualitatively by the Coulomb interaction between electrons and holes, but the reason why the maximum resonance occurs at a slightly higher energy than that of the hole excitation seen in Raman scattering is presently unknown.³³ This is an area where more theoretical work is needed.

VII. CONCLUDING REMARKS

In the present paper, we used an effective-mass description of electrons and holes in self-assembled quantum dots, and computed, by means of exact-diagonalization techniques, the wave functions of initial (ground), intermediate, and final states entering the transition amplitude of an inelastic light-scattering process, Eq. (1). Polarized and depolarized Raman cross-sections in the backscattering geometry for dots with electron numbers $N_e = 2 - 6$, and harmonic confinement strengths $\hbar\omega_e = 20 - 50$ meV were calculated. The role of collective (charge and spin-density excitations) and single-particle excitations in Raman spectra was stressed. Particularly interesting is the case of open-shell dots, where the spin selection rules do not hold for Raman scattering, and the 6-electron dot, where an almost idealized Raman process with transition through a single intermediate resonance can be realized. We found evidence of approximate outgoing resonances in our second-order scheme, without the need of higher-order terms in the scattering amplitude. Existing experimental results were qualitatively analysed, although their proper description requires further work, for example, on the inclusion of the polaron effect in Raman scattering.

Acknowledgments

Part of this work was performed using the computing facilities of the Abdus Salam ICTP, Trieste, Italy. The authors acknowledge helpful discussions with B. Aslan and support by the Caribbean Network for Quantum Mechanics, Particles and Fields (ICTP) and by the Programa Nacional de Ciencias Basicas (Cuba).

-
- ¹ C. Schuller, *Inelastic Light Scattering of Semiconductor Nanostructures* (Springer, Berlin, 2006).
 - ² L. Chu et. al., *Appl. Phys. Lett.* 77, 3944 (2000).
 - ³ T. Brocke, M.-T. Bootsmann, M. Tews, et. al., *Phys. Rev. Lett.* 91, 257401 (2003).
 - ⁴ B. Aslan, H.C. Liu, M. Korkusinski, et. al., *Phys. Rev. B* 73, 233311 (2006); *J. Nanosci. Nanotechnol.* 8, 789 (2008).
 - ⁵ O. Verzelen, R. Ferreira, G. Bastard, *Phys. Rev. Lett.* 8, 146803 (2002).
 - ⁶ E. Menendez-Proupin, C. Trallero-Giner, and S.E. Ulloa, *Phys. Rev. B* 60, 16747 (1999).
 - ⁷ C.P. Garcia, V. Pellegrini, A. Pinczuk, et. al., *Phys. Rev. Lett.* 95, 266806 (2005).
 - ⁸ S. Kalliakos, M. Rontani, V. Pellegrini, et. al., *Nature Phys.* 4, 467 (2008).
 - ⁹ A. Gonzalez and A. Delgado, *Physica E* 27, 5 (2005).
 - ¹⁰ O. Madelung, *Semiconductors: Data Handbook* (Birkhauser, Stuttgart, 2004).
 - ¹¹ R. Loudon, *Adv. Phys.* 13, 423 (1964).
 - ¹² A. Delgado, A. Gonzalez, and D.J. Lockwood, *Phys. Rev. B* 69, 155314 (2004).
 - ¹³ A. Delgado, *Inelastic Light Scattering by Electronic Excitations in Artificial Atoms*, Ph. D. thesis, Institute of Cybernetics, Mathematics and Physics, Havana (2006).
 - ¹⁴ L. Jacak, P. Hawrylak, and A. Wojs, *Quantum Dots* (Springer, Berlin, 1998).
 - ¹⁵ Z.R. Wasilewski, S. Fafard, and J.P. McCaffrey, *J. Crystal Growth* 201/202, 1131 (1999).
 - ¹⁶ P. Hawrylak and M. Korkusinski, in P. Michler (Ed.), *Single Quantum Dots* (Springer, Berlin, 2003), *Topics Appl. Phys.* 90, 25 (2003).
 - ¹⁷ M. Rontani, C. Cavazzoni, D. Belluci, and G. Goldoni, *J. Chem. Phys.* 124, 124102 (2006).
 - ¹⁸ S. Kvaal, arXiv:0810.2644.
 - ¹⁹ P. Ring and P. Schuck, *The Nuclear Many-Body Problem* (Springer-Verlag, New-York, 1980).
 - ²⁰ A. Delgado, A. Gonzalez and E. Menendez-Proupin, *Phys. Rev. B* 65, 155306 (2002).
 - ²¹ J.K. Cullum and R.A. Willoughby, *Lanczos Algorithms for Large Symmetric Eigenvalue Computation* (Birkhauser, Stuttgart, 1985).
 - ²² A. Delgado, A. Gonzalez, and D.J. Lockwood, *Solid State Commun.* 135, 554 (2005).
 - ²³ This fact was already noticed for closed shell (relatively large) etched dots in A. Delgado, A. Gonzalez, and D.J. Lockwood, *Phys. Rev. B* 71, 241311 (2005).
 - ²⁴ G. Danan, A. Pinczuk, J.P. Valladares, et al, *Phys. Rev. B* 39, 5512 (1989).
 - ²⁵ R. Strenz et al., *Phys. Rev. Lett.* 73, 3022 (1994).
 - ²⁶ D.J. Lockwood et al., *Phys. Rev. Lett.* 77, 354 (1996).
 - ²⁷ C. Schuller et al., *Phys. Rev. Lett.* 80, 2673 (1998).
 - ²⁸ C. Steinebach, C. Schuller, and D. Heitmann, *Phys. Rev. B* 59, 10240 (1999).
 - ²⁹ C. Steinebach, C. Schuller, and D. Heitmann, *Phys. Rev. B* 61, 15600 (2000).
 - ³⁰ B. Aslan, private communication.
 - ³¹ S. Kalliakos et al., *Nano Lett.* 8, 577 (2008).
 - ³² D. Bougeard et al., *Physica E* 21, 312 (2004).
 - ³³ B. Aslan et al., *Electr. Lett.* 43, 1162 (2007).